

Topological and Orbital-Based Mechanisms of the Electronic Stabilization of Bis(Diisopropylamino)Cyclopropenyldiene

Lucius E. Johnson[†] and Donald B. DuPré*

Department of Chemistry, University of Louisville, Louisville, Kentucky 40292

Received: March 13, 2008; Revised Manuscript Received: May 22, 2008

Previous analysis of the topology of the electron density of bis(dimethylamino)cyclopropenyldiene as a model of the stable bis(diisopropylamino)cyclopropenyldiene revealed mechanisms of induction/back-polarization, σ -aromaticity, and σ - π polarization to be responsible for the electronic stabilization of the divalent carbon C2 upon amino substitution on the 3MR. This work presents new data from molecular orbital calculations and a full analysis of the operative natural bond orbitals and their interactions. The discrepancies between these orbital-based stabilization mechanisms and the physical stabilization based upon the quantum theory of atoms in molecules are uncovered through the separation of electron localization and delocalization indices into contributions from orbitals of σ - and π -symmetry, as well as calculated nucleus-independent chemical shifts that determine the degree of σ - and π -delocalization/aromaticity. Graphical representations of functions of the electron density mapped onto various π -orbital isosurfaces serve to better visualize the underlying differences between mathematical orbital space and the real space of the electron density. This work also provides new insight into the topological-based mechanism through investigation of the changes in the virial of the electronic forces acting on the interatomic surfaces—forces that govern the bonding and stabilization within a molecule.

I. Introduction

In an earlier paper,¹ we reported the mechanism of electronic stabilization of the three-membered ring (3MR) and carbene carbon (C2) of the recently synthesized² and stable bis(diisopropylamino)cyclopropenyldiene (**3** in Scheme 1) to involve inductive effects of the electronegative planar nitrogen substituents with subsequent back-polarization^{3,4} (not back-donation) of the electron density in the 3MR. The plane-perpendicular lone pairs, $n_{\pi}(\text{N})$, of nitrogen utilize *in*-plane σ -aromaticity^{5–8} in the ring as a conduit to delocalize charge toward the C2 carbon. There, for the singlet carbene, σ - π polarization^{9–11} acts to preferentially push charge into the π -plane, partially filling in the depletion gap responsible for the electrophilic character of the ambiphilic C2, stabilizing **3** in regard to dimerization with respect to the parent cyclopropenyldiene compound, H_2C_3 (**1**). This work, based solely on the topology of the electron density of the molecule obtained using the quantum theory of atoms in molecules (QTAIM),^{3,12} presented a very different picture of the stabilization mechanism than that of the orbital model (Scheme 1) which suggests $n_{\pi}(\text{N})$ and $\pi(\text{C}=\text{C})$ conjugation and $n_{\pi}(\text{N}) \rightarrow p_{\pi}^*(\text{C}2)$ hyperconjugation with the formally empty $p_{\pi}^*(\text{C}2)$ orbital as the source of nonsteric stabilization.

Here, we will present a full analysis of the cyclopropenyldiene systems of the parent compound **1** and an abbreviated model **2**, where $\text{R} = \text{NMe}_2$, of **3**. This includes results of molecular orbital (MO), natural bond orbital (NBO), canonical molecular orbital (CMO), natural chemical shielding (NCS), and nucleus-independent chemical shift (NICS) calculations. The findings will be compared to the QTAIM-derived mechanisms previously reported,¹ as well as with new calculations of interatomic surface virials.^{3,13,14} These atomic virials describe the balance of forces

within the molecule that leads to the bonding force holding atoms together (as opposed to MO-based "bonds", which are not physically measurable quantities).^{14,15} The disparity between the two methods is revealed by analysis of the atomic overlap matrix (AOM). Localization and delocalization indices, calculated from the AOM, can be separated into contributions from σ - and π -orbitals, allowing a connection between orbital-based terminology and calculated atomic properties. The root of the difference between the orbital and topological approaches is also highlighted through graphical representation of quantities calculated.

II. Methods Section

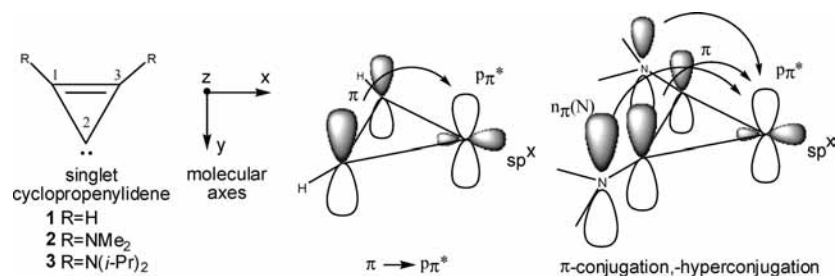
The equilibrium geometries of the molecules of this study were fully optimized, and normal-mode frequency analysis was performed, using density functional theory (DFT) at B3LYP/6-31G(d,p),^{16,17} as implemented in Gaussian03.¹⁸ The coordinates of all optimized models of this study are found in the Supporting Information for our previous paper.¹

The resultant electron density, ρ , obtained from the wave function of all optimized structures was analyzed with the quantum theory of atoms in molecules (QTAIM)³ using the AIM2000 program¹⁹ with wave functions generated with Gaussian03.¹⁸ Atomic overlap matrices (AOM) were obtained by integration of the MO overlap matrix over the respective atomic basins, and the localization index of atomic basin A, $\lambda(\text{A})$, and the delocalization index between atoms A and B, $\delta(\text{AIB})$, were calculated from the AOM, as described by Fradera et al.²⁰ and Biegler-König and Schönbohm.¹⁹ Due to the planar symmetry of the molecules of this study, the AOM may be separated into contributions from orbitals of σ - and π -symmetry as they are orthogonal and have no overlapping terms.¹⁹ Likewise, the σ - and π -orbital contributions to the localization and delocalization indices were calculated. Interatomic surface

* To whom correspondence should be addressed. E-mail: d.dupre@louisville.edu.

[†] E-mail: lejohn07@louisville.edu.

SCHEME 1



integrations using AIM2000 yielded the total virial of the force (VoF) on the interatomic surface as well as the VoF on each side of the surface.

NBO,²¹ NRT,²² CMO, and NCS²³ calculations were performed on the optimized structures using NBO 3.1,²⁴ as implemented in Gaussian03, and NBO 5.0.²¹ Second-order perturbation energies, $E2$, for donor-acceptor orbital interactions were calculated, and in cases where $E2$ is large, the NBO deletion energy, $E(\text{del})$, of that specific interaction was calculated.

NICS²⁵ magnetic shielding calculations were performed using the gauge-including atomic orbital (GIAO)^{26,27} method at the B3LYP/6-31g(d,p)^{16,17} level of theory in Gaussian03.¹⁸ Ghost atoms were placed at 0 and 1 Å above the ring critical point (RCP). The σ - and π -orbital contributions to the individual components of the NICS tensors were obtained through NCS calculations with NBO 5.0.^{21,23} NICS(r) values are defined as the negative of the isotropic magnetic shielding at a distance r above the ring critical point; NICS_{zz, σ (r), for example, refers to the contribution from the σ -orbitals to the NICS value resulting from a z -applied magnetic field.}

Plots of MO isosurfaces were created using GaussView 3.0²⁸ with cube files generated with Gaussian03.¹⁸ Values of the electron density, ρ , and the Laplacian of the electron density were mapped onto the MO isosurfaces using the respective cube files.

III. Results and Discussion

1. Natural Bond Orbitals. Each in-plane NBO of the ring carbons of **1** and **2** shows a decrease in electronic population upon amino substitution (see Table 1). The $\sigma(\text{C2-C1})$ and the identical $\sigma(\text{C2-C3})$ σ -bonding orbitals each lose 0.032 electrons, even though the bonds are shorter, 1.430 Å for R = H and 1.414 Å for R = NMe₂. (In what follows, only the properties of one of any pair of symmetrically identical NBOs, such as $\sigma(\text{C2-C1})$ and $\sigma(\text{C2-C3})$, will usually be discussed.) The $\sigma(\text{C1-C3})$ σ -bond loses 0.028 electrons, and the one-center lone-pair orbital $n(\text{C2})$ on C2 loses 0.026 electrons. While the $\pi(\text{C1-C3})$ π -bond orbital experiences a loss of 0.082 electrons, the other π -plane orbitals show large gains in electron density. The formally “empty” $p\pi^*$ orbital on singlet C2 gains 0.187 electrons, and the $\pi^*(\text{C1-C3})$ orbital gains 0.341 electrons. All of these changes corroborate the orbital-based viewpoint that amino substitution leads to in-plane σ -induction accompanied by out-of-plane π -back-donation by the nitrogen atoms. The net result is a decrease of charge in the σ -plane and an increase in the π -plane.

Second-order perturbation energies ($E2$) provide a measure of energy lowering in the system through delocalization of charge from occupied donor orbitals into unoccupied acceptor orbitals.²¹ The interaction is a function of the spatial overlap of the two specific orbitals, the energy difference between the two, and the electron population of the donor orbital. If $E2$ is large,

TABLE 1: Natural Bond Orbital (NBO) Populations in e and Second-Order Perturbation Energies ($E2$) in kcal/mol for Cyclopropenyldienes (R = H, NMe₂)

NBO	R = H	R = NMe ₂
$\sigma(\text{C1-C2})$	1.941	1.909
$\sigma(\text{C1-C3})$	1.983	1.955
$n(\text{C2})$	1.990	1.964
$p\pi^*(\text{C2})$	0.408	0.595
$\pi(\text{C1-C3})$	1.592	1.510
$\pi^*(\text{C1-C3})$	0	0.341
$n_{\pi}(\text{N})$	—	1.716
$E2$ (kcal/mol)		
$\sigma(\text{C1-C2}) \rightarrow \sigma^*(\text{C3-H,N})$	36.06 ^a	48.38 ^a
$\pi(\text{C1-C3}) \rightarrow p\pi^*(\text{C2})$	121.14 ^a	139.48 ^a
$n_{\pi}(\text{N}) \rightarrow \pi^*(\text{C1-C3})$	—	46.64 ^a
$n_{\pi}(\text{N}) \rightarrow p\pi^*(\text{C2})$	—	1.56
Geminal Interactions		
$\sigma(\text{C1-C2}) \rightarrow \sigma^*(\text{C2-C3})$	4.73	4.21
$\sigma(\text{C1-C2}) \rightarrow \sigma^*(\text{C1-C3})$	8.63	9.01
$\sigma(\text{C1-C3}) \rightarrow \sigma^*(\text{C1-C2})$	4.39	5.78
$\sigma(\text{C1-C3}) \rightarrow \sigma^*(\text{C2-C3})$	4.34	5.78
$\sigma(\text{C2-C3}) \rightarrow \sigma^*(\text{C1-C2})$	4.69	4.21
$\sigma(\text{C2-C3}) \rightarrow \sigma^*(\text{C1-C3})$	8.66	9.00
sum (geminal interactions)	35.44	37.99

^a $E(\text{del})$ NBO deletion energies. See the Methods Section for details.

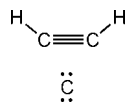
higher-order perturbation terms cannot be ignored. In this case, the deletion energy, $E(\text{del})$, of the interaction needs to be calculated. The interaction of the donor $\sigma(\text{C2-C1})$ σ -bond through the ring center to the acceptor $\sigma^*(\text{C3-N})$ antibond is strongly stabilizing, with $E(\text{del}) = -36.06$ and -48.38 kcal/mol for R = H and R = NMe₂, respectively. The increase in this interaction energy is due to the increase in polarization of the opposed $\sigma^*(\text{C3-N})$ antibonding orbital around C3 and into the ring center, allowing for a larger overlap with the $\sigma(\text{C2-C1})$ bond.

The $E(\text{del})$ energy of the $\pi(\text{C1-C3}) \rightarrow p\pi^*(\text{C2})$ lone pair interaction increases from -121.14 kcal/mol when R = H to -139.48 kcal/mol when R = NMe₂. Even though the population of the $\pi(\text{C1-C3})$ π -bond decreases by 0.082 electrons, the energy difference between the orbitals decreases by 8.39 kcal/mol, and the spatial overlap increases due to the shorter $\sigma(\text{C2-C1})$ and $\sigma(\text{C2-C3})$ bonds. The $\pi(\text{C1-C3}) \rightarrow p\pi^*(\text{C2})$ delocalization is coupled with strong $n_{\pi}(\text{N}) \rightarrow \pi^*(\text{C1-C3})$ donations that stabilize the molecule, with $E(\text{del}) = -43.64$ kcal/mol for each $n_{\pi}(\text{N}) \rightarrow \pi^*(\text{C1-C3})$ interaction. The $E2$ interaction energy for the $n_{\pi}(\text{N}) \rightarrow p\pi^*(\text{C2})$ donation, the supposed hyperconjugation that adds stability when R = NMe₂, is rather low, with the $E2 = -1.56$ kcal/mol. The majority of the electronic stabilization of C2 would appear to come from the $\pi(\text{C1-C3}) \rightarrow p\pi^*(\text{C2})$ interaction. The population of the $p\pi^*(\text{C2})$ NBO increases from 0.408 electrons when R = H to

0.595 electrons when $R = \text{NMe}_2$. This results in a filling in of the orbital susceptible to nucleophilic attack and a lessening of the propensity of the molecule to dimerize. However, from the NBO perspective, the electronic stability of the entire ring system that arises from amino substitution is not from the $n_\pi(\text{N}) \rightarrow p_\pi^*(\text{C}2)$ hyperconjugations but mainly from the increase in the through-ring $\sigma(\text{C}2-\text{C}1) \rightarrow \sigma^*(\text{C}3-\text{N})$ and $\sigma(\text{C}2-\text{C}3) \rightarrow \sigma^*(\text{C}1-\text{N})$ interactions and out-of-plane $\pi(\text{C}1-\text{C}3) \rightarrow p_\pi^*(\text{C}2)$ donations, with the addition of the stabilizing $n_\pi(\text{N}) \rightarrow \pi^*(\text{C}1-\text{C}3)$ delocalizations.

NBO calculations on cyclopropane²⁹ show several stabilizing factors that overcome the strain of the 3MR. The decrease in the $\angle\text{CCC}$ angles adds more p-character to the ring carbon bond hybrids, thus weakening the bonds. However, the decreased angle allows for a sharp increase in the overlap of one ring $\sigma(\text{C}-\text{C})$ bond orbital with a geminal $\sigma^*(\text{C}-\text{C})$ antibond, thus increasing the geminal stabilization in the 3MR relative to unstrained analogues. The NBO bonds do bend outward from the ring carbon lines-of-center, but a significant amount of the bond density is still found inside of the ring. This is the NBO counterpart of surface delocalization (σ -aromaticity). Also, the increased p-character of the ring bonds leads to a stabilizing increase in the s-character of the *exo*- $\sigma(\text{C}-\text{H})$ bond orbitals.

We also calculated the *E2* perturbation energies for the geminal stabilizations for **1** and **2**, as well as the NRT resonance contributors to the overall structure. As seen in Table 1, the sum of the six geminal *E2* energies of the 3MR increases upon R-substitution, totaling -35.44 kcal/mol when $R = \text{H}$ and -37.99 kcal/mol when $R = \text{NMe}_2$. The p-character of the carbon ring hybrids decreases when $R = \text{NMe}_2$, increasing the stabilization of the 3MR. The *exo* hybrids of the ring carbons—those in the $\sigma(\text{C}-\text{N})$ bonds and the $n(\text{C}2)$ lone pair—see a slight resultant increase in p-character. No significant resonance structures, such as the one depicted below, showing ring-plane “ π -complex” structures suggested by Dewar³⁰ for cyclopropane, were found in our NRT calculations on cyclopropenylidene.



2. Canonical Molecular Orbitals. The main instability of singlet carbenes in the laboratory lies in their tendency to dimerize or polymerize.³¹ The parent cyclopropenylidene **1** is present in outer space due to the low frequency of self-interaction² but tends to polymerize in the laboratory. As shown in Table 2, when $R = \text{H}$, the LUMO is the $\pi^*(\text{C}1-\text{C}3)$ orbital, not the empty $p_\pi^*(\text{C}2)$ orbital, predicting polymerization rather than dimerization when reacting with the lone pair $n(\text{C}2)$ HOMO of another molecule. When $R = \text{NMe}_2$, the LUMO is predominantly the $p_\pi^*(\text{C}2)$ orbital. The synthesized cyclopropenylidene **3** is of course also sterically protected from dimerization by the bulky isopropyl groups. The theoretical model **2** offers only electronic protection that is reflected in the calculated increase (Table 2) in the HOMO–LUMO gap of $+28.8$ kcal/mol compared to the parent compound **1**. This makes **2**, and by extension **3**, inherently less reactive.

3. Comparison with Analysis of the Topology of the Electron Density and QTAIM Properties. The orbital analysis above has shown increased out-of-plane and through-ring delocalizations and an increase in the HOMO–LUMO gap to be the main electronic stabilizing factors upon amino substitution

TABLE 2: Calculated Molecular Orbital Energies and HOMO–LUMO Gap in kcal/mol and MO Isosurface Plots for Cyclopropenylidenes

molecular orbital	energy (kcal/mol)	
HOMO $R = \text{H}$	−140.50	
HOMO $R = \text{NMe}_2$	−114.96	
LUMO $R = \text{H}$	−16.13	
LUMO $R = \text{NMe}_2$	−38.22	
HOMO–LUMO gap		
$R = \text{H}$	124.37	
$R = \text{NMe}_2$	153.18	

of the cyclopropenylidene ring. Our previous paper¹ presented the QTAIM analysis of the topology of the electron density, where it was found that the effect of the electronegative nitrogen atoms is to first exert an inductive drawing of charge away from C1 and C3. To maintain the stability of these atoms, the electron density of the atomic basins is back-polarized and consequently pushes charge into the σ -bond paths of the ring carbons. This is a compensatory effect that is necessary to maintain the zero-flux condition ($\nabla\rho(r) \cdot \mathbf{n}(r) = 0$, where $\mathbf{n}(r)$ is a unit vector normal to the surface) defining the boundaries of the atomic basins and to prevent an abnormal rise in the energy of the C1(C3) carbon atoms. The nitrogen atoms are planar and show $n_\pi(\text{N})$ lone-pair-like, nonbonded valence shell charge concentrations (VSCCs) above and below the molecular plane. A detailed analysis of the change in the ellipticity along the N–C1(C3) bond paths showed that the major axis (direction of the λ_2 eigenvector) rotates from the π -plane into the σ -plane well before reaching the nuclei of C1 and C3.¹ The $n_\pi(\text{N})$ lone pairs thus are able to participate in surface delocalization (σ -aromaticity) of the 3MR, carrying charge to C2 preferentially in the σ -plane. Charge is also preferentially concentrated in the σ -plane of the formal C1–C3 double bond; however, the ellipticity $\varepsilon(\text{C}1-\text{C}3) = 0.18$ at the BCP is unusually low for a double bond. The delocalization is complete in the basin of C2 where charge is pushed into the π -plane (σ – π polarization) to relieve Coulomb repulsion, resulting in a partial filling in of the $p_\pi^*(\text{C}2)$ gap. This redounds on the reactivity of the molecule as it reduces the nucleophilic exposure of C2 and impedes dimerization.

We can reconcile these two conflicting viewpoints by analyzing the atomic overlap matrix (AOM) that is a part of QTAIM calculations.^{19,20} The separation of the AOM into σ - and π -orbital contributions will clarify where (in the σ - or in the π -plane of the molecule) the electron density is distributed and localized and what the orbital pathways are for electron delocalization. Table 3 shows the breakdown of the localization and delocalization indices into these σ - and π -contributions.

TABLE 3: Electron Localization $\lambda(A)$ and Delocalization $\delta(A|B)$ Indices, σ - and π -Orbital Contributions, and Changes in the Indices From $R = H$ to $R = NMe_2$ [$\Delta(NMe_2-H)$], Calculated from the Atomic Overlap Matrices for Cyclopropenylidenes

localizations	R = H	R = NMe ₂	$\Delta(NMe_2-H)$
$\lambda(C1)$	4.141	3.620	-0.521
$\lambda(C1) \sigma$	3.834	3.266	-0.568
$\lambda(C1) \pi$	0.308	0.354	0.046
$\lambda(C2)$	4.580	4.566	-0.014
$\lambda(C2) \sigma$	4.499	4.362	-0.137
$\lambda(C2) \pi$	0.082	0.205	0.123
$\lambda(H,N)^a$	0.380	6.375	5.995
$\lambda(H,N) \sigma$	0.380	4.960	4.580
$\lambda(H,N) \pi$	0.000	1.415	1.415
delocalizations	R = H	R = NMe ₂	$\Delta(NMe_2-H)$
$\delta(C1 C2)$	1.279	1.260	-0.019
$\delta(C1 C2) \sigma$	0.962	0.902	-0.060
$\delta(C1 C2) \pi$	0.317	0.358	0.041
$\delta(C1 C3)$	1.693	1.382	-0.311
$\delta(C1 C3) \sigma$	1.078	1.025	-0.053
$\delta(C1 C3) \pi$	0.615	0.357	-0.258
$\delta(C2 H,N)^a$	0.051	0.124	0.073
$\delta(C2 H,N) \sigma$	0.045	0.073	0.028
$\delta(C2 H,N) \pi$	0.006	0.052	0.046
$\delta(C1 H,N)^a$	0.943	1.100	0.157
$\delta(C1 H,N) \sigma$	0.933	0.831	-0.102
$\delta(C1 H,N) \pi$	0.011	0.269	0.258

^a Indices involving H for cyclopropenylidene 1 and N for 2.

Delocalization between C1(C3) and C2 shifts slightly from the σ - to the π -plane relative to $R = H$, which agrees with the calculated¹ slight decrease in the in-plane ellipticity of the electron density along the C1(C3)–C2 bond paths. However, the delocalization, like the ellipticity, is still predominantly in the σ -plane of the molecule—confirmation of the dominance of σ -aromaticity over π -delocalization. The small delocalization index $\delta(N|C2) = 0.124$ between the nitrogens and C2 is also σ -plane dominated. This coincides with the preferential distribution of electron density in the plane, as reported in our previous paper.¹ The delocalization along the N–C1 and N–C3 bond paths is also dominated by the σ -contribution, although there is some π -contribution. The latter is indicative of π -back-donation, though not to the extent of that predicted by the $n_\pi(N) \rightarrow \pi^*(C1-C3)$ NBO deletion energy. The decrease in the $\pi(C1-C3)$ NBO population of **2** relative to **1** is mirrored by the decrease in $\delta_\pi(C1|C3)$ of -0.258 ; both decreases are due to the preferential withdrawal by nitrogen of higher-energy, less tightly held π -electrons. All of the increases in the π -contributions to the localization indices also mirror the increases seen in the Q_{zz} atomic quadrupole tensor components discussed in our previous paper.¹

σ -Localized charge in the atomic basin of C1(C3) is lost to nitrogen due to induction, as expected. Relative to $R = H$, localized charge at C2 decreases in the σ -plane ($\Delta\lambda_\sigma(C2) = -0.137$) and increases in the π -plane ($\Delta\lambda_\pi(C2) = +0.123$). The increase in π -localization at C2 might be taken to confirm the orbital-based mechanisms of π -conjugation and π -hyperconjugation. The decrease in the σ -localization of C2 would then be due to the loss of σ -electrons from C2 through induction by the electron-depleted C1(C3) carbons. However, as will be shown below, the orbital-based mechanisms do not hold up in the face of evidence derived from further calculations of the properties of the electron density and the physical forces that govern the geometry, energetics, and properties of the molecule.

TABLE 4: Calculated QTAIM Properties of Cyclopropenylidenes: Bond Path Length (R_b), Density (ρ_b), Laplacian ($\nabla^2\rho_b$), and Ellipticity (ϵ) at the Bond Critical Point (BCP), Delocalization Index $\delta(C1|C2)$, and Virial of the Force (VoF) on the Interatomic Surface (IAS) Between C1(C3) and C2, and Atomic Charges of C1(C3) and C2^a

	R = H	R = NMe ₂
R_b	1.435	1.421
$\delta(C1 C2)$	1.279	1.260
ρ_b	0.281	0.287
$\nabla^2\rho_b$	-0.542	-0.580
ϵ (BCP) ellipticity	0.60	0.39
C2 atomic charge	0.09	-0.02
C1(C3) atomic charge	-0.13	0.37
total VoF exerted on C1 C2 IAS	-0.2044	-0.2622
VoF exerted on C1 side of IAS	-0.1752	-0.2302
VoF exerted on C2 side of IAS	-0.0292	-0.0320

^a AIM properties in atomic units (au); R_b in Å.

4. Virial of the Forces Exerted on the Interatomic Surfaces. Bonding between pairs of atoms, A and B, occurs because the attractive forces of electrons of one atom for the nucleus of the other are greater than the repulsive forces between the electrons and between the respective nuclei. If the electron–nuclear force is such to draw the atoms together, then there will be a negative (attractive) potential energy density on the A|B interatomic surface.^{13,14} In the stationary state, nuclear–nuclear and electron–electron repulsions are balanced by these attractive forces.

With the inductive withdrawal of electrons by nitrogen, we would expect greater attraction of the C2 electrons for the exposed C1(C3) nucleus. If this were the source of the decrease in $\lambda_\sigma(C2)$, then the force of attraction of the electrons of C2 for the C1(C3) basins would be increased—the virial of the force (VoF) on the C2 side of the C2|C1(C3) surface would become more negative. However, it is the VoF on the C1(C3) side of the surface that increases in magnitude, from -0.1752 when $R = H$ to -0.2302 when $R = NMe_2$. The VoF on the C2 side changes little (see Table 4). The inductive effect by nitrogen on the C1(C3) charge results in back-polarization, pushing charge against the C1(C3) side of the interatomic surface with C2 and bringing about the increase in the VoF. Furthermore, back-polarized C1(C3) charge density near the C2|C1(C3) surface subsequently shields the C1(C3) nucleus from an increased attractive force from the C2 electrons. Thus, the VoF on the C2 side of the surface only changes from -0.0292 when $R = H$ to -0.0320 when $R = NMe_2$.

5. Visualization of the Discrepancy Between Orbital-Based and Electron-Density-Based Mechanisms. MOs are often used to visualize electron density distributions and delocalizations and to explain mechanisms of molecular stabilization and/or reactivity. This would seem to stem from the desire to ground our understanding of the physics of chemistry in a spatially visual concept. The misconception of electrons being evenly distributed within balloon-shaped orbitals is (understandably) introduced in the high school chemistry classroom and constantly modified throughout undergraduate courses as students develop a more complete understanding. In many situations, the orbital-based predictions of molecular properties match well with observations, and their utility in the understanding and prediction of spectroscopic properties is undeniable.¹⁴ However, when looking at the reactivity and properties of any molecule, it is the distribution of negatively charged electrons about positively charged nuclei that determines the attractive (bonding) forces within the molecule, the suscep-

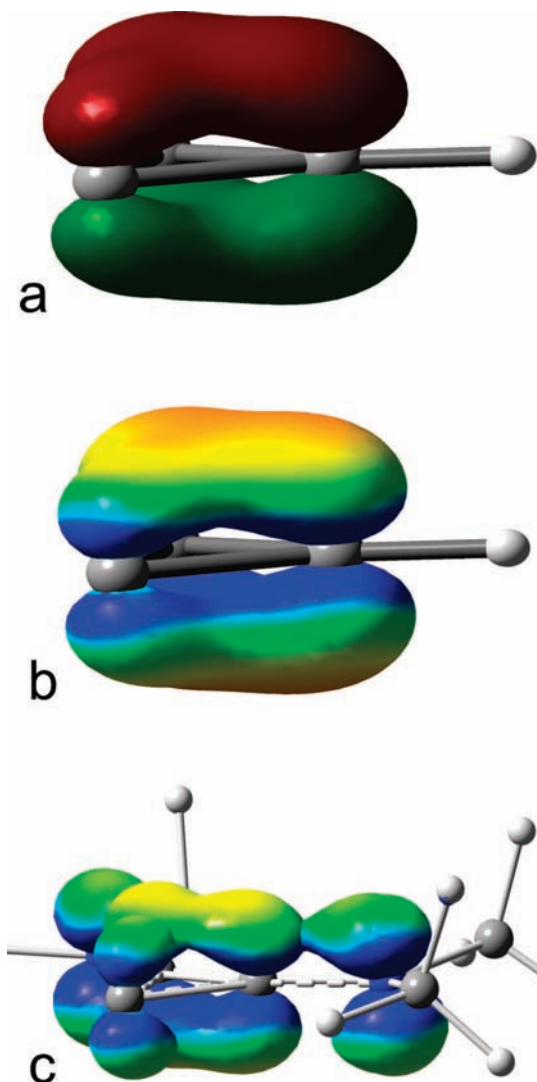


Figure 1. Isosurfaces of π -MOs for (a) and (b) $R = H$ (MO 8) and (c) $R = NMe_2$ (MOs 30, 32, 33) at 0.1 au. In b and c, the electron density function is mapped onto the MO isosurface. The surface color scales from density values of 0 (red, charge depletion) to 0.2 (blue, charge concentration).

tibility of the molecule to electrophilic or nucleophilic attack, and the energetics of the system. MOs are used computationally to generate a molecular wave function, but it is the topology of the total electron density, whether calculated from the wave function or obtained experimentally, that determines the properties of the molecule.^{3,14,15}

The recent boom of the development of stable, isolable carbenes^{32,33}—previously only pictured as reaction intermediates—seems to beg for a better, more thorough understanding of the actual mechanism of electronic stabilization. The following plots serve to visualize the difference between the orbital-based and electron-density-based points of view for the cyclopropenylidene models of this study.

The π -MO for cyclopropenylidene **1** extends well out-of-plane (see Figure 1a) and recalls the concept of $\pi(C1-C3) \rightarrow p_{\pi}^*(C2)$ delocalization. It contains considerable contribution from all three ring carbons. CMO calculations show the MO to contain 80% $\pi(C1-C3)$ and 20% $p_{\pi}^*(C2)$ character. What is not apparent from either Figure 1a or from MO calculations is *where* the electron density is distributed within the MO. Figure 1b,c helps visualize what was discovered in the investigation of the localization and delocalization indices discussed above.

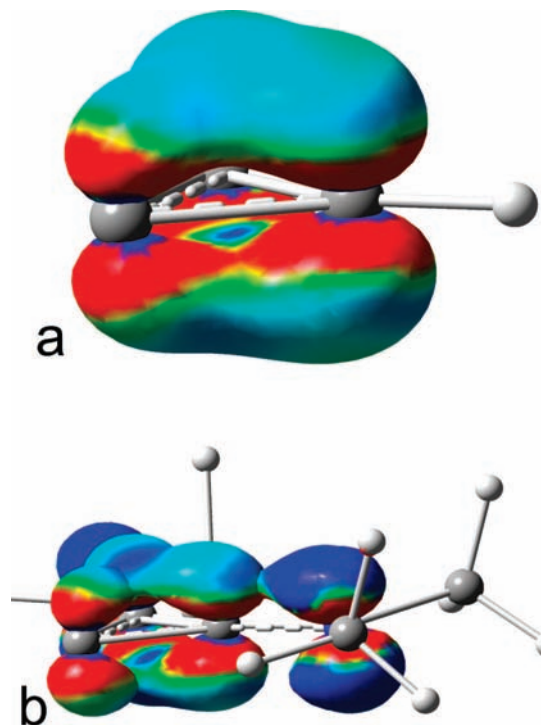


Figure 2. Laplacian of the electron density, $\nabla^2\rho$, mapped onto the 0.1 au isosurfaces of the π -MOs for (a) $R = H$ and (b) $R = NMe_2$. The surface color scales from Laplacian values of -0.2 (red, charge concentration) to $+0.2$ (blue, charge depletion).

The shading of the MO isosurface indicates the value of the electron density at each point on the surface, where blue indicates higher charge concentration. As seen by the region of dark blue on the MO surface, charge density is preferentially distributed in the area close to the molecular plane, rather than being spread out evenly throughout the MO.

The Laplacian of the electron density, $\nabla^2\rho$, is mapped onto the same MO isosurfaces in Figure 2a,b. In this case, the red areas on the surfaces for both **1** and **2** indicate larger concentrations of electron density that are mostly situated in the vicinity of the ring carbons. Again, charge is found to be preferentially distributed throughout the σ -plane, not the π -plane of the MO. Dark blue surfaces indicate charge depletion in the ring centers, rather than π -delocalization across the ring.

Figure 3a,b sheds light on the large $E(\text{del})$ values for the $\pi(C1-C3) \rightarrow p_{\pi}^*(C2)$ interaction. The “bubble” between the C1 and C3 atoms in the $\pi(C1-C3)$ isosurface is from the $p_{\pi}^*(C2)$ NBO encroaching on the surface and delineates the overlap of the two orbitals. The dark blue surface in the region of the overlap indicates a region of considerable charge depletion.

6. NMR and Nucleus-Independent Chemical Shift (NICS).

In our previous paper,¹ the mechanisms of C2 and ring stabilization when $R = NMe_2$ were corroborated by the properties of calculated NMR shielding tensors. Here, we investigate how the changes in σ/π localization and delocalization lead to changes in the magnetic response of the system by using the NICS²⁵ method as a probe for σ - and/or π -aromatic effects. Once again due to symmetry, the NICS values may be broken down into contributions that arise separately from σ - and π -MO-induced current density.

In the small ring cyclopropenylidene system, the isotropic shielding at the ring center is dominated by the paramagnetic currents induced by the in-plane magnetic field components that rotate nonbonding density at C2 into the zone of valence shell

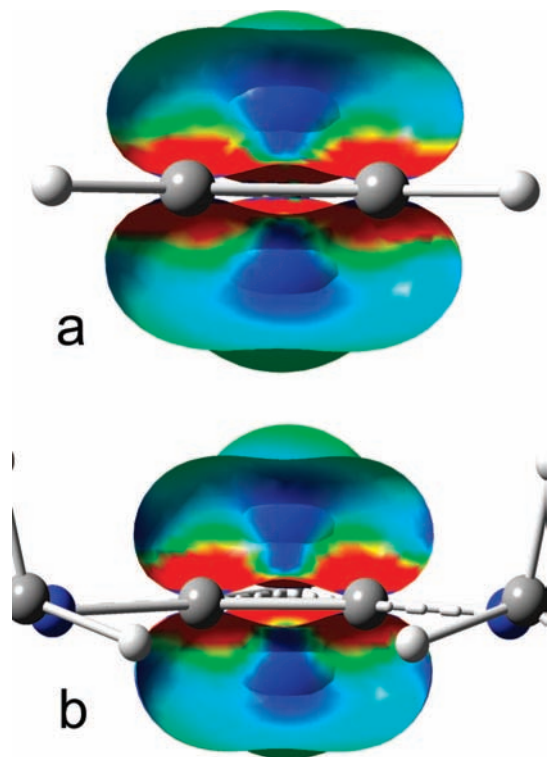


Figure 3. Laplacian of the electron density, $\nabla^2\rho$, mapped onto the 0.1 au isosurfaces of the $\pi(\text{C1-C3})$ and $p_{\pi}^*(\text{C2})$ NBOs for (a) $\text{R} = \text{H}$ and (b) $\text{R} = \text{NMe}_2$. The viewpoint is from behind the C1-C3 bond looking toward C2. The $\pi(\text{C1-C3})$ NBO surface is cut to see the inside of the surface and the overlapping $p_{\pi}^*(\text{C2})$ NBO. The surface color scales from Laplacian values of -0.2 (red, charge concentration) to $+0.2$ (blue, charge depletion).

depletion above and below the plane. Any changes in the ring currents upon R substitution are masked. Therefore, investigation of the out-of-plane component of the NICS tensors (NICS_{zz}) should provide a better understanding of the magnetic response to the changes in the electron density distribution throughout the ring.²⁵ As a reminder, $\text{NICS}(r)$ is defined as the negative of the shielding at point r . A negative NICS value indicates delocalization/aromaticity as the induced currents act to oppose the applied magnetic field and thus shield at point r . If electron density is not delocalized and there is a low-lying orthogonal virtual orbital, then electrons can unpair and align with the applied magnetic field, serving to deshield the area.

$\text{NICS}_{zz}(0)$ values listed in Table 5 show the presence of both σ - and π -aromaticity in the ring. However, the predominance of σ -aromaticity can be clearly seen. When $\text{R} = \text{H}$, $\text{NICS}_{zz,\pi}(0) = -12.70$, while $\text{NICS}_{zz,\sigma}(0) = -27.86$. Both of these indicators of aromaticity decrease slightly in magnitude when $\text{R} = \text{NMe}_2$ due to lower electron density and less delocalization within the ring. If there were increased π -conjugation and delocalization when $\text{R} = \text{NMe}_2$, as suggested by the orbital viewpoint, then this should lead to increased shielding currents (and a more negative NICS value) induced by the out-of-plane (z) magnetic field component. However, the $\text{NICS}_{zz,\pi}(r)$ value actually decreases in magnitude when $\text{R} = \text{NMe}_2$ at both $r = 0$ (at the RCP) and 1 (1 Å above the RCP, used to remove any effects from ring plane concentration). This slight decrease in the π -delocalization indicator is a result of the decrease in π -electron delocalization and increase in π -localization in the ring carbons upon R substitution as calculated from the AOM.

TABLE 5: Nucleus-Independent Chemical Shift Values, $\text{NICS}(r)$, at a Distance (r), Å, Above the RCP for Cyclopropenyldienes, Out-of-Plane Component [$\text{NICS}_{zz}(r)$] Values, and σ -Orbital [$\text{NICS}_{\sigma}(r)$] and π -Orbital [$\text{NICS}_{\pi}(r)$] Contributions

	at RCP	$\text{R} = \text{H}$	$\text{R} = \text{NMe}_2$
$\text{NICS}(0)$		-15.86	-34.24
$\text{NICS}_{\pi}(0)$		-26.37	-23.68
$\text{NICS}_{\sigma}(0)$		10.51	-10.56
$\text{NICS}_{zz}(0)$		-40.57	-36.74
$\text{NICS}_{zz,\pi}(0)$		-12.70	-11.47
$\text{NICS}_{zz,\sigma}(0)$		-27.86	-25.27
1 Å above RCP			
$\text{NICS}(1)$		-16.67	-13.94
$\text{NICS}_{\pi}(1)$		-4.42	-2.21
$\text{NICS}_{\sigma}(1)$		-12.25	-11.73
$\text{NICS}_{zz}(1)$		-31.36	-20.45
$\text{NICS}_{zz,\pi}(1)$		-11.30	-10.02
$\text{NICS}_{zz,\sigma}(1)$		-20.06	-10.43

IV. Conclusions

Our previous paper¹ presented a mechanism of 3MR and divalent carbon stabilization contradictory to the orbital-based mechanism shown in Scheme 1. NBO and MO calculations reveal extensive π -delocalization as the main stabilizing factor upon amino substitution of the parent cyclopropenyldiene. This is evident by the increase in the $p_{\pi}^*(\text{C2})$ population and the increase in the $E2$ and $E(\text{del})$ stabilizing π -delocalization energies. However, further investigation with QTAIM calculations, visualization of properties of the electron density, and NICS calculations all serve to support the actual physical mechanisms of 3MR and C2 stabilization upon amino substitution. The effect of nitrogen substitution is two-fold. The lone-pair-like charge concentrations of the nitrogen atoms above and below the molecular plane rotate into the molecular plane so as to participate in the σ -aromaticity of the 3MR. The inductive power of nitrogen also withdraws charge from neighboring C1 and C3 atomic basins, resulting in back-polarization of the remaining C1(C3) electron density toward C2. This causes an increase in the virial of the force on the C1(C3) side of the C2|C1(C3) interatomic surface. The electron density of the 3MR is preferentially distributed in the σ -plane of the ring, and the delocalization indices are all dominated by contributions from orbitals of σ -symmetry. The back-polarization of charge in the σ -plane causes σ - π polarization of the nonbonding valence charge of C2, pushing charge into the π -plane. The decrease in σ -localized charge and subsequent increase in π -localized charge in the C2 atomic basin reduces the exposure of C2 to nucleophilic attack, thus electronically stabilizing **2**, and by extension **3**, relative to the parent molecule **1**. The discrepancy between the orbital and topological mechanisms is highlighted by the mapping of the electron density and its Laplacian onto isosurfaces of the π -MOs and π -NBOs of the molecules. Charge density is not evenly distributed throughout the out-of-plane orbitals and is actually seen to be preferentially concentrated near and in the ring plane. This includes a notable lack of concentration of charge in the areas of NBO donor-acceptor orbital overlap that presumably leads to the increased π -delocalization when $\text{R} = \text{NMe}_2$. Finally, using NICS calculations as a gauge of charge delocalization and its magnetic response, the predominance of σ -aromaticity over π -delocalization is confirmed, even upon amino substitution of the parent cyclopropenyldiene.

Acknowledgment. Supercomputer time allocations received from the National Computational Science Alliance and from the Advanced Biomedical Computing Center of the Frederick Cancer Research and Development Center, National Institutes of Health, are acknowledged. Support for this work also came from a Research Initiation Grant from the Office of the Vice President for Research, University of Louisville, and an Intramural Research Grant from the College of Arts and Sciences, University of Louisville. A NSF-DGE (GK-12) graduate fellowship to L.E.J. is gratefully acknowledged.

Supporting Information Available: Complete author list for ref.¹⁸ This material is available free of charge via the Internet at <http://pubs.acs.org>.

References and Notes

- (1) Johnson, L. E.; DuPré, D. B. *J. Phys. Chem. A* **2007**, *111*, 11066–11073.
- (2) Lavallo, V.; Canac, Y.; Donnadiou, B.; Schoeller, W. W.; Bertrand, G. *Science* **2006**, *312*, 722–724.
- (3) Bader, R. F. W. *Atoms in Molecules. A Quantum Theory*; Clarendon Press: Oxford, U.K., 1990.
- (4) Bader, R. F. W.; MacDougall, P. J.; Lau, C. D. H. *J. Am. Chem. Soc.* **1984**, *106*, 1594–1605.
- (5) Dewar, M. J. S. *J. Am. Chem. Soc.* **1984**, *106*, 669–682.
- (6) Cremer, D. *Tetrahedron* **1988**, *44*, 7427–7453.
- (7) Cremer, D.; Kraka, E. *J. Am. Chem. Soc.* **1985**, *107*, 3800–3810.
- (8) Cremer, D.; Gauss, J. *J. Am. Chem. Soc.* **1986**, *108*, 7467–7477.
- (9) Wiberg, K. B.; Hadad, C. M.; Breneman, C. M.; Laidig, K. E.; Murcko, M. A.; LePage, T. J. *Science* **1991**, *252*, 1266–1272.
- (10) Bader, R. F. W.; Chang, C. J. *J. Phys. Chem.* **1989**, *93*, 5095–5107.
- (11) Wiberg, K. B.; Rosenberg, R. E.; Rablen, P. R. *J. Am. Chem. Soc.* **1991**, *113*, 2890–2898.
- (12) Popelier, P. *Atoms in Molecules. An Introduction*; Prentice Hall: New York, 2000.
- (13) Bader, R. F. W.; Fang, D. C. *J. Chem. Theory Comput* **2005**, *1*, 403–414.
- (14) Bader, R. F. W. *Monatsh. Chem.* **2005**, *136*, 819–854.
- (15) Bader, R. F. W. *Int. J. Quantum Chem.* **2003**, *94*, 173–177.
- (16) Becke, A. D. *J. Chem. Phys.* **1993**, *98*, 5648–5652.
- (17) Lee, C.; Yang, W.; Parr, R. G. *Phys. Rev.* **1988**, *B37*, 785–789.
- (18) Frisch, M. J. et al. *Gaussian03*, revision C.02; Gaussian, Inc.: Wallingford, CT, 2004.
- (19) Biegler-Konig, F.; Schonbohm, J. *J. Comput. Chem.* **2002**, *23*, 1489–1494.
- (20) Fradera, X.; Austen, M. A.; Bader, R. F. W. *J. Phys. Chem. A* **1999**, *103*, 304–314.
- (21) Glendening, E. D.; Badenhop, J. K.; Reed, A. E.; Carpenter, J. E.; Bohmann, J. A.; Morales, C. M.; Weinhold, F. *NBO 5.0 Program Manual. Natural Bond Orbital Analysis Programs, NBO 5.0. Theoretical Chemistry Institute, University of Wisconsin: Madison, WI, 2001.*
- (22) (a) Glendening, E. D.; Weinhold, F. *J. Comput. Chem.* **1998**, *19*, 593–609. (b) Glendening, E. D.; Weinhold, F. *J. Comput. Chem.* **1998**, *19*, 610–627. (c) Glendening, E. D.; Badenhop, J. K.; Weinhold, F. *J. Comput. Chem.* **1998**, *19*, 628–646.
- (23) Bohnmann, J. A.; Weinhold, F.; Farrar, T. C. *J. Chem. Phys.* **1997**, *107*, 1173–1184.
- (24) Glendening, E. D.; Reed, A. E.; Carpenter, J. E.; Weinhold, F. *NBO Version 3.1 Program Manual. Theoretical Chemistry Institute and Department of Chemistry, University of Wisconsin: Madison, WI, 1990.*
- (25) Chen, Z.; Wannere, C. S.; Corminboeuf, C.; Puchta, R.; Schleyer, P. v. R. *Chem. Rev.* **2005**, *105*, 3842–3888, and references therein.
- (26) Ditchfield, R. *Mol. Phys.* **1974**, *27*, 789–807.
- (27) Wolinski, K.; Hinton, J. F.; Pulay, P. *J. Am. Chem. Soc.* **1990**, *112*, 8251–8260.
- (28) Dennington I. I., Roy, Keith., Todd; Millam, John; Eppinnett, Ken.; Hovell, W. Lee.; and Gilliland, Ray. *GaussView*, version 3.09; Semichem, Inc.: Shawnee Mission, KS, 2003.
- (29) Weinhold, F.; Landis, C. *Valency and Bonding; A Natural Bond Orbital Donor–Acceptor Perspective*; Cambridge University Press: Cambridge, U.K., 2005; pp 270–275.
- (30) Dewar, M. J. S.; Ford, G. P. *J. Am. Chem. Soc.* **1979**, *101*, 783–791.
- (31) Reisenauer, H. P.; Maier, G.; Riemann, A.; Hoffmann, R. W. *Angew. Chem., Int. Ed. Engl.* **1984**, *23*, 641.
- (32) Bourissou, D.; Guerret, O.; Gabbai, F. P.; Bertrand, G. *Chem. Rev.* **2000**, *100*, 39–91.
- (33) Canac, Y.; Soleilhavoup, M.; Conejero, S.; Bertrand, G. *J. Organomet. Chem.* **2004**, *689*, 3857–3865.

JP802214U